Physica A 391 (2012) 4909–4922

Contents lists available at SciVerse ScienceDirect

Physica A

journal homepage: www.elsevier.com/locate/physa

Fractal descriptors based on Fourier spectrum applied to texture analysis

João Batista Florindo, Odemir Martinez Bruno *

Instituto de Física de São Carlos (IFSC), Universidade de São Paulo (USP), Av. Trabalhador São Carlense, 400, 13560-970 - São Carlos, SP, Brazil

ARTICLE INFO

Article history:
Received 15 October 2011
Received in revised form 18 March 2012
Available online 9 May 2012

Keywords:
Fractal descriptors
Fractal dimension
Fractal multiscale
Fourier spectrum

ABSTRACT

This work proposes the development and study of a novel technique for the generation of fractal descriptors used in texture analysis. The novel descriptors are obtained from a multiscale transform applied to the Fourier technique of fractal dimension calculus. The power spectrum of the Fourier transform of the image is plotted against the frequency in a log–log scale and a multiscale transform is applied to this curve. The obtained values are taken as the fractal descriptors of the image. The validation of the proposal is performed by the use of the descriptors for the classification of a dataset of texture images whose real classes are previously known. The classification precision is compared to other fractal descriptors known in the literature. The results confirm the efficiency of the proposed method.

1. Introduction

Although studies of fractal objects have been underway for more than a century, it is in the last decades that a growing number of works have been presented in literature, showing applications of fractals in several branches of science. The fractals demonstrate the ability in the representation overall of objects found in nature, as already attested in Ref. [1]

Following this idea, one can find the work of several authors [2,38,39] demonstrating the viability of a fractal dimension method in the calculus of the fractal dimension of non fractal objects. Works like [1,2] and others encouraged the development of works describing natural objects by the fractal dimension [3–5]. These works experimented with a lot of techniques for the extraction of image features based on fractal geometry and more specifically on methods for the calculus of fractal dimension, like Minkowski sausage [6], Fourier [7], etc.

Extending the concept of fractal dimension, [8] presents the concept of multiscale fractal dimension, in which the fractal dimension is calculated at different scales of observation, allowing the obtainment of a set of numbers called the descriptors of the analyzed object, allowing for the enrichment of this sort of analysis. Plotze et al. [3] applied this concept, using the Minkowski sausage method, and obtained interesting results in the task of classification of Brazilian plants, based on the digitalized images of their leaves. Backes et al. [9] also applied the fractal descriptors to the analysis of texture images and provided good results.

The present work proposes the development and study of a novel multiscale fractal descriptor for texture images. Here, the descriptors are obtained from the Fourier method for the fractal dimension calculus. In the Fourier technique, the fractal dimension is calculated from the power law detected in the graph of the power spectrum as a function of the frequency in the Fourier transform of the image. When this graph is plotted in a bi-log scale, the curve is approximately similar to a straight line and the dimension is provided by the slope of such line.

The idea in this work is the application of a multiscale transform to the whole curve in log–log scale to provide the descriptors for the original image. In order to verify the power of the proposed technique in the description of texture images,

* Corresponding author. Tel.: +55 16 3373 8728; fax: +55 16 3373 9879.
E-mail addresses: florindo@ursa.ifsc.usp.br (J.B. Florindo), bruno@ifsc.usp.br (O.M. Bruno).

0378-4371/$ – see front matter © 2012 Elsevier B.V. All rights reserved.
doi:10.1016/j.physa.2012.03.039

the descriptors obtained are used in a process of classification of these images. The performance of the novel technique is validated by the comparison with other fractal descriptors known in the literature. We chose to compare only fractal analysis methods, as the literature presents several works showing the efficiency of fractal analysis faced with conventional texture analysis technique in natural image analysis [11–15,3,16,9,10].

This work is divided into 8 sections. In the next, we show a brief study about fractal geometry. The third section presents the Fourier fractal dimension. The fourth one describes fractal descriptors. In the fifth section, the proposed technique is described. The following section describes the experiments performed with the aim of validating the proposed technique. The seventh section shows the results. The eighth section expresses the conclusions of the work.

2. Fractal geometry

Roughly speaking, a fractal is an object characterized by an infinite self-similarity and an infinite complexity. The self-similarity means that whether we observe a specific part of the object, this part behaves like a copy (or "quasi-copy") of a greater or smaller part of the same object and this process is repeated at any observation scale taken. In its turn, the concept of complexity lacks a precise definition, but may be understood as the level of detail observed at each different observation scale.

The most important measure used in the characterization of a fractal entity is its fractal dimension defined initially in Ref. [1]. This value estimates the spatial occupation of the fractal as well as its self-similarity degree.

Mandelbrot [1] uses the Hausdorff–Besicovitch measure as the fractal dimension. The Hausdorff–Besicovitch dimension dim_H of a metric space X is given by:

$$dim_H(X) = \inf\{d \geq 0 | C_H^d(X) = 0\},$$

where $C_H^d(X)$ is the d-dimensional Hausdorff content of X, defined by:

$$C_H^d(X) = inf \sum_i r_i^d | \text{there exists a cover of x using balls of radii } r_i > 0$$

Particularly, in the case of self-similar objects as the fractals, a simpler expression for the calculus of Hausdorff–Besicovitch dimension D, directly based on the calculus of the Euclidean topological dimension and called the similarity dimension, is given by:

$$D = \lim_{u \to 0} \frac{lnN}{lnL/u},$$

where N is the number of "units" u needed to cover the whole extension L of the object.

The above formula gave rise to the development of a lot of computational methods for the calculus of the fractal dimension of fractals represented as discrete objects in a digital image, which simplified significantly the obtainment of this measure. The methods used for the fractal dimension calculus in these cases may be essentially divided into two categories: the spatial methods, like box-counting [18], Bouligand–Minkowski [6] and mass-radius [18] and the spectral methods, like Fourier [7] and wavelets [19]. Here, we focus on the Fourier method for the calculus of the fractal dimension and this approach is described more minutely in the next section.

3. Fourier fractal dimension

The fractal dimension of an object can be calculated through the Fourier transform associated to a mass distribution $\mu(u)$, $u \in \Re^n$ and by using a classical Physics analogy. Let the Fourier transform of μ thus be defined through:

$$\tilde{\mu(u)} = \int_{\Re^n} e^{ix*u} d\mu(x).$$

In classical Physics, we have the definition of the s-potential ϕ_s, $s \geq 0$ of the mass distribution μ by:

$$\phi_s(x) = \int \frac{d\mu(y)}{|x-y|^s}.$$

In the same way, the s-energy I_s is obtained through:

$$I_s(\mu) = \int \phi_s(x) d\mu(x).$$

Applying these concepts to the mass distribution μ:

$$\phi_x(x) = (|.|^{-s} * \mu) \equiv \int |x-y|^{-s} d\mu(y).$$

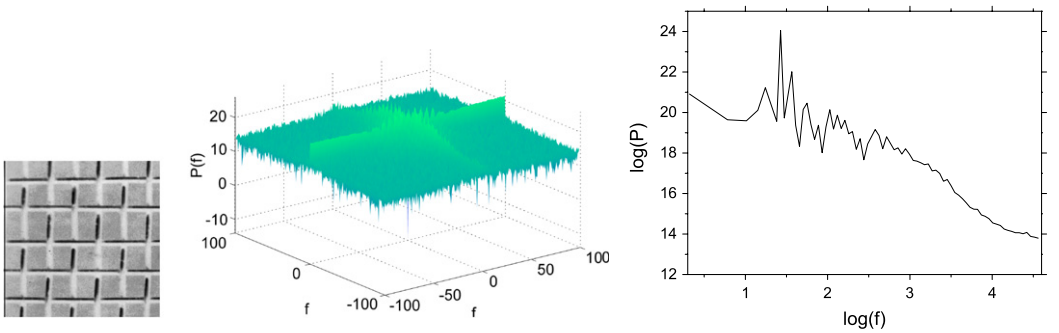

Fig. 1. Steps in fractal dimension calculus by Fourier method for texture images from two different classes. On the left, the original texture. At the center, the Fourier spectrum. On the right, the plot of spectrum × frequency.

Performing the Fourier transform and using the convolution theorem:

$$\tilde{\phi}_s(x) = c|u|^{s-n}\tilde{\mu}(u).$$

From Parseval's theorem, we thus have:

$$I_s(\mu) = (2\pi)^n c \int \hat{\phi}_s(u)\overline{\tilde{\mu}(u)}du.$$

The energy is in this way easily obtained through:

$$I_s(\mu) = (2\pi)^n c \int |u|^{s-n}|\hat{\mu}(u)|^2 du. \tag{1}$$

The Hausdorff dimension of C has its lower limit in s if there is a mass distribution μ on the set $C \in \Re^2$ for which the expression (1) is finite. Still, if $|\tilde{\mu}(u)| \leq b|u|^{-t/2}$, for a real constant b, then $I_s(\mu)$ always converges if $s < t$. The greatest t for which there is a mass distribution μ on C is called the Fourier fractal dimension of C.

Based on the mathematical theory, [7] proposes the use of the Fourier transform, more precisely, the power spectrum of the transform as a tool for the calculus of fractal dimension of texture images. Russ [7] shows that the average Fourier power spectrum of the texture image obeys a power law scaling as described in Ref. [1].

The power law is verified between the power spectrum F_h and the frequency f and is expressed by:

$$F_h \propto f^{2-\beta_h},$$

where β_h is the exponential parameter [7].

As a consequence of the power law, the plot in a log–log scale of the graph of $F_h x f$ results in a curve whose behavior approximates that of a straight line. Russ [7] shows that the Fourier fractal dimension FD_h of the image can be calculated by

$$FD_h = \frac{6+\beta_h}{2},$$

where β_h is the slope of the straight line best fitted to the curve in log–log scale. It is noticeable that the slope of this straight line at different directions is approximately constant, demonstrating the isotropism of the original image, allowing the application of Fourier fractal dimension calculus. The Fig. 1 illustrates the process applied to 4 texture images (from 2 different classes).

4. Fractal descriptors

With the popularization of computer-aided image analysis techniques, an increase in the amount of data processed by the computational algorithms was also observed. Such a fact led to the development of techniques with the aim of extracting relevant information in each image. The values encapsulating this essential information were called image descriptors and described important features from objects represented in the image.

Specifically, in texture analysis, a classical use of descriptors is the use of the Fourier descriptors [20], a reduced set of values describing the whole texture image which in its original format was meaningless for a classification algorithm, for example. The literature still showed the development of more robust descriptors, as Gabor [21] and wavelets [22], among others.

Mandelbrot [1] and other authors [2,7] observed that many objects found in nature present characteristics intrinsic to fractals, like the self-similarity and advanced levels of complexity. Such observations motivated authors like [19,5,4] to employ the fractal dimension concept as a descriptor for objects of the real world, represented in images.

Extending this idea, [8] suggested the use of not only the fractal dimension as a unique descriptor but a set of values extracted from the fractal dimension measure process to characterize an image. Finally, [16] formalized the concept of fractal descriptors as being a set of values extracted from fractal geometry methods and used to characterize artifacts in an image, like textures, contours, shapes, etc. We may still see examples of applications of fractal descriptors in Ref. [3,9,23,17], among others.

Particularly, in this work, we present a novel method for fractal descriptors based on the fractal dimension calculated by using the Fourier spectrum of the image, described in the Section 3.

5. Proposed method

Following the idea of the aforementioned works, here we propose the development of a novel fractal descriptor for texture images. We explore the obtainment of a set of descriptors by applying a multiscale approach to the technique of fractal dimension calculus by Fourier transform. Thus, we initially define the concept of multiscale transform.

5.1. Multiscale transform

In practical situations, often we are faced with the need to analyze signals or images presenting different structures and patterns at different observation scales. In order to capture such scale variance, [24] proposed the development of multiscale transform. Still, a lot of works [8,25,26] applied the multiscale transform for the analysis of experimental data in different situations.

Essentially, the multiscale transform of a signal $u(t)$ is the function $U(b, a)$, where b is directly associated with t and a is the scale variable. Roughly speaking, the multiscale transform may be accomplished through three approaches: scale-space, time–frequency, time-scale. Each approach is briefly described in the following. More details may be seen in Ref. [18].

5.1.1. Scale-space

Scale-space transform is the most used multiscale transform. It is based on Gaussian kernel properties [24] and may be expressed by the following expression:

$$\{(b, a)|a, b \in \Re, a > 0, b \in \{U^1(t, a)\}_z c\},$$

where $\cdot_z c$ denotes the zero-crossings of the expression $\cdot$ and $U^1(t, a)$ expresses the convolution of the original signal $u(t)$ with the first derivative of the Gaussian g_a^1, that is:

$$U^1(t, a) = u(t) * g_a^1(t).$$

5.1.2. Time-frequency

Witkin [24] demonstrates that the scale a and the frequency f are simply related through $a = 1/f$. This result allows for the use of frequency transforms in multiscale approaches. Specifically, the time–frequency transform is based on the short-time Fourier transform, using a Gaussian kernel. The following expression summarizes the transform:

$$U(b, f) = \int_{-\infty}^{+\infty} g * (t - b)u(t)e^{-i2\pi ft}dt,$$

where $g*$ is the conjugate of the classical Gaussian. In practice, the transform is performed through Gabor filters [18].

5.1.3. Time-scale

Finally, we have the time-scale transform, in which the slide window used in the short-time Fourier transform for time–frequency transform has variable side length allowing a better precision in the frequency localization. In this context, we notice that wavelet transform [18] is the best candidate for the calculus of such particular transform. Thus, the time-scale transform may be represented through:

$$U\Phi(b, a) = \frac{1}{\sqrt{(a)}} \int_R \Phi * \left(\frac{t - b}{a}\right) u(t)dt,$$

where Φ is the classical mother wavelet and $*$ denotes its conjugate.

5.2. Extracting information from the multiscale transform

A particular aspect of multiscale transform is that it maps a one-dimensional signal onto a two-dimensional function, resulting in information redundancy. In order to solve such a drawback the literature showed some proposals. For instance, [27] proposed the use of local maxima, minima and zeros of the transform $U(b, a)$. Rosin and Venkatesh [28] used the projection of $U(b, a)$ onto the scale (equivalent to frequency) axis. Finally, [29] presented the use of a specific scale a_0.

In this work, we opted for the analysis of the multiscale transform of Fourier fractal dimension through the last approach, selecting a specific scale. Such a choice was motivated by the fact that we cannot prioritize any region of log–log curve in our application, once the fractal characteristic is sensibly altered, if we do not take into account the whole curve.

As described in detail in the Section 3, the Fourier fractal dimension is calculated by the slope of a straight line fitted to the curve of power spectrum × frequency in the log–log scale. The method used to calculate the Fourier fractal dimension presents an inherent multiscale characteristic given by the use of the frequency as a scale variable. As demonstrated in Ref. [24], in a multiscale analysis, frequency and scale are two ways of expressing the same property. In fact, by the Fourier filtering theory [18], we know that the lower frequencies express a general "view" of the image while the higher express more detailed structures in the original image. In order to emphasize this multiscale aspect, we propose the application of a multiscale transform to the curve in log–log scale.

In its turn, the inherent constitution of image textures implies that these textures contain relevant information stored in specific patterns of fine and coarse structures (more and less detailed). This is a strong motivation for the use of the fractal dimension being an interesting tool to describe such textures, quantifying the degree of complexity (details) at different scales of observation.

In addition to this, the use of the multiscale transform applied to the fractal dimension allows for a richer description of this complexity pattern of the image. Instead of using the unique value of fractal dimension, with the multiscale transform, we obtain a curve with a set of values, which represents in a more faithful manner the original texture, by expressing not only the complexity of texture as a whole but measuring the complexity at each different scale.

Based on this assumption, [8] studied the extraction of multiscale features from the fractal dimension and used such features in a genic expression problem, obtaining interesting results. Plotze et al. [3] and [16] applied the scale-space transform to the Bouligand–Minkowski fractal dimension and used the generated values as descriptors in a shape recognition task. Backes et al. [9] used the multiscale transform of Bouligand–Minkowski in a texture recognition problem.

All these works applying multiscale to the fractal dimension presented in the literature demonstrated the accuracy of this approach in image analysis, presenting an advantage over the classical methods used for this purpose. With this in mind, here we propose a novel multiscale fractal approach, comparing it with other known fractal descriptor approaches. For the generation of descriptors, we propose the application of a multiscale transform over the curve of $\log(powerspectrum) \times \log(frequency)$ described in Section 3. Based on empirical verifications we opted for the use of scale-space transform. The Fig. 2 exemplifies that such descriptors can differentiate textures extracted from two different scenes (classes).

5.3. Compared fractal dimensions

We may find a lot of fractal dimension estimation methods. Here, we choose those which are more correlated to the application of the proposed technique, that is, the texture analysis. It is important to emphasize that all these methods estimate the same theoretical fractal dimension. In the following, we show a brief description of each one. The reader can find more details in each cited reference.

5.3.1. Box-counting

This is a three dimensional adaptation of the conventional box-counting fractal dimension [35]. In this approach, initially, we map the gray-level image $I \in [1 : M] \times [1 : N] \to \Re$ onto the surface S, in such a way that each pixel with coordinate (x, y) in the image is mapped onto a point in the 3D space with coordinates (x, y, z), where z is the pixel intensity, that is:

$$S = \{i, j, f(i, j) | (i, j) \in [1 : M] \times [1 : N]\}, \tag{2}$$

and

$$f(i, j) = \{1, 2, \ldots, \max\_I\} | f = I(i, j), \tag{3}$$

where $\max\_I$ corresponds to the maximum gray intensity in the image.

In the following, the space surrounding S is divided into grids of cubes with a variable side-length r. For each r value used, we count the number $N(r)$ of cubes which contain at least one point of S. The fractal dimension D_{BC} is estimated through the following log–log relation:

$$D_{BC} = \lim_{r \to 0} \frac{\log(N(r))}{\log(r)}.$$

In practice, this value is obtained by plotting the function $r \times N(r)$ in a log–log scale and fitting a straight line to the curve. The dimension is provided by the slope of such line.

Here, we used the whole interval of values in $N(r)$ in order to capture the multiscale relation intrinsic to the estimation method and provide a fairer comparison to the proposed novel technique.

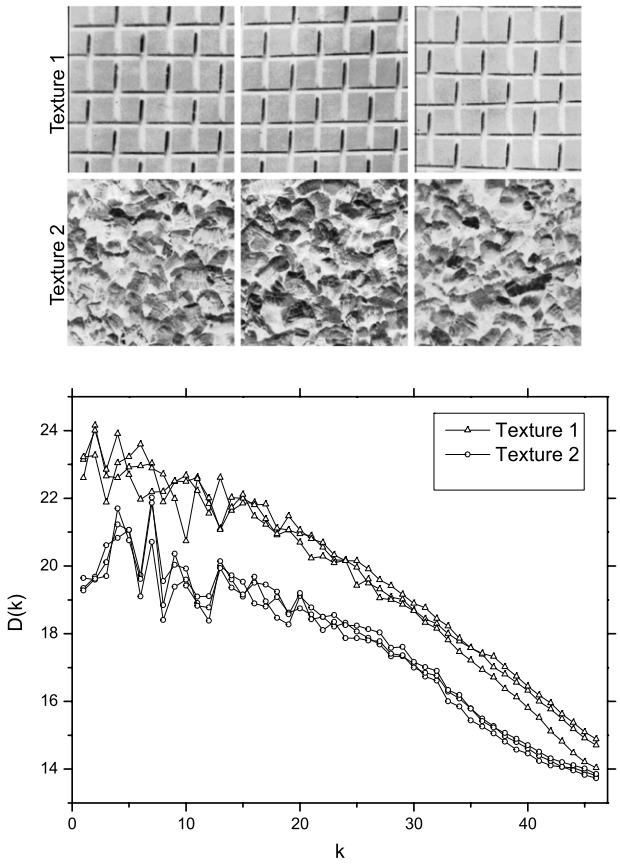

Fig. 2. Fourier fractal descriptors $D(k)$ of textures extracted from different classes.

5.3.2. Bouligand–Minkowski

In the fractal dimension estimation of gray-level images by the Bouligand–Minkowski method [9], we also start with the mapping of such an image into a 3D surface S in the same manner used in the box-counting technique.

Thus, this surface is dilated by a sphere with variable radius r. The dilation consists essentially of drawing a sphere with radius r and centered at each point the surface S. The number of points contained in the union of such spheres is called the dilation volume $V(r)$. The Bouligand–Minkowski dimension D_{BM} is computed by the following:

$$D_{BM} = \lim_{r \to 0} \frac{\log(V(r))}{\log(r)}.$$

This limit is calculated in the same manner as that employed in the box-counting technique, that is, it corresponds to the slope of a straight line fit to the curve $r \times V(r)$ represented in log–log scale.

In the comparison, we also used the whole $V(r)$ curve. The multiscale is implicit in the dilation process. A thinner sphere captures more details while a greater sphere radius suggests a more global view of the image surface.

5.3.3. Brownian motion

The essential idea of this method is to assume that an image approximates the behavior of a Brownian motion distribution, that is, the probability distribution of neighbor pixel intensities has mean 0 and a variance which grows exponentially with the distance.

In practice, we may estimate the fractal dimension of an image $I : N \times N \to \Re$ of gray-level intensity from the following exponential relation:

$$D = \lim_{k \to 0} \frac{\log(id(k))}{\log(k)},$$

where $id(k)$ is given through the following expression:

$$id(k) = \left(\begin{array}{l} \displaystyle\sum_{x=0}^{N-1}\sum_{y=0}^{N-k-1} (I(x,y) - I(x,y+k))/(N(N-k)) + \\ \displaystyle\sum_{y=0}^{N-1}\sum_{x=0}^{N-k-1} (I(x,y) - I(x+k,y))/(N(N-k)) + \\ \displaystyle\sum_{x=0}^{N-k-1}\sum_{y=0}^{N-k-1} (I(x+k,y) - I(x,y+k))/(N(N-k)) + \\ \displaystyle\sum_{x=0}^{N-k-1}\sum_{y=0}^{N-k-1} (I(x,N-y) - I(x+k,N-y-k))/(N(N-k)) \end{array} \right) \Big/ 4.$$

Here, we used the whole curve $id(k)$ in the comparison with the proposed method. More details on the implementation may be found in Ref. [34].

5.3.4. Variation dimension

This method is similar in some sense to the two dimensional version of box-counting. The digital image is divided into a grid of boxes with side length r. Thus for each value of r we estimate the variation $D(r)$ as being the sum of differences between the maximum and minimum intensity of the image inside each box. The dimension is computed from the following relation:

$$D_V = \lim_{r\to 0} \frac{\log(D(r))}{\log(r)}.$$

The limit is estimated through the straight line fit in the same manner as for the previous methods. More details may be seen in Ref. [44].

5.3.5. Multifractal spectrum

The calculus of multifractal spectrum [36] also involves the initial mapping of the image I onto a surface S. In the following, we device S into a grid of cubes, in the same way as in the box-counting technique. Thus, we apply an integer label i to each cube. We have N_i points of S in the box i. In this way, we define the mass probability $\mu_i = N_i/N$, where N is the total number of points in S. Based on this, we may define a measure M by:

$$M_d(q,\delta) = \lim_{\delta\to 0}\lim_{\delta\to 0}\sum_i \mu_i^q \delta^d = \lim_{\delta\to 0} N(q,\delta)\delta^d.$$

The measure $M_d(q,\delta)$ is 0 when $d > \tau(q)$ and ∞ when $d < \tau(q)$.

The multifractal spectrum itself is finally obtained through the expression:

$$D(q) = \frac{1}{q-1}\cdot\lim_{\delta\to 0}\frac{\log\sum_i \mu_i^q}{\log\delta} = \frac{1}{q-1}\cdot\lim_{\delta\to 0}\frac{\log N(q,\delta)}{\log\delta}, \quad \text{for } q \neq 1 \text{ and}$$

$$D(q) = -\lim_{\delta\to 0}\frac{\sum_i \mu_i \log\mu_i}{\log\delta}, \quad \text{for } q = 1.$$

5.3.6. Other fractal measures

Regarding their importance in the literature, we also compare the results to other classical measures, that is, the regularization dimension [41–43,40] and the lacunarity. In these cases, we used the direct implementation present in the FracLab software [45,46].

6. Experiments

The validation of the proposed technique is implemented by means of a classification experiment of datasets of texture images whose classes are predetermined.

The experiments are executed over four texture datasets. The first is the classical texture dataset of Brodatz [30], complete with 10 windows extracted from each texture sample, constituting in this way 111 classes with 10 samples in each class. The second dataset is composed by textures of real scenarios and is named USPTex. This dataset is composed by 191 classes with 12 images in each class. The third one is the OuTex dataset [31] for tests. This is composed by 68 classes with 20 natural texture images in each class. Finally, we used a plant leaves data set [9], composed by images from the leaf texture of different Brazilian plant species. This data consists of 10 classes with 200 samples in each class.

The classification is properly executed by the Bayesian classifier technique [32] implemented in weka environment [33]. The Bayesian method was chosen since, although it obtains lower correctness rates in the classification process, it corresponds to an optimal classifier and is less susceptible to particular characteristics of each compared descriptor or dataset. The accuracy of the classification is compared to other descriptor methods found in the literature and based on the fractal theory, that is, fractal Brownian motion, box-counting, Bouligand–Minkowski volumetric fractal descriptors and multifractal probability spectrum. We also compare to three fractal measures well-known in the literature, they are, regularization and variation dimension and lacunarity. We compare the global correctness rate of each descriptor and the behavior of each method varying the number of descriptors.

We opted to compare only fractal methods due to the scope of this work which emphasizes texture fractal analysis. Moreover, the literature shows a lot of works comparing and demonstrating the power of fractal analysis face of classical texture analysis methods. The interested reader may, for instance, consult such a comparison in works like [11–15,3,16,9,17].

Relative to the number of descriptors, an important aspect to be stated is that in the fractal approach we do not limit the number of descriptors according to the number of samples per class. This procedure suggested in works like [37] is fundamental when descriptors are a set of features. Nevertheless, in fractal analysis, the set of descriptors must be thought of as a unique correlated feature with a multiple dimension. Even the results in the next section show that the use of a reduced set of fractal descriptors compromises seriously the performance of the method.

7. Results

The Fig. 3 exhibits the correctness rate (percentage of images correctly classified) when varying the number of descriptors used in the Brodatz dataset. We observe that most descriptors have a similar global aspect, presenting a huge variation with few descriptors and tending to stabilize when the number of descriptors increases. Such behavior is justifiable by the nature of such methods, in which the first descriptors capture more faithfully the nuances in the object, in this case, the surface representing the texture image. In the box-counting experiment, the number of descriptors is limited by log_2^N, where N is the side length of the image, once for each descriptor the side length of the box is doubled. The correctness rate also presents an exponential growing as the number of descriptors grows. Finally, the proposed technique presents a relation approximately linear of the correctness relative to the number of descriptors. Such an appearance of the curve was weighted, due to the linear nature of the Fourier transform.

It is important to point out that although other methods present better results than Fourier when using few descriptors, the correctness tends to stabilize from a certain number of descriptors. This fact is explained by the so-called curse of dimensionality. In its turn, the Fig. 4 shows the curves of correctness rate relative to the number of descriptors in the USPTex dataset. The global aspect of curves is similar to that seen in the Fig. 3. Nevertheless, the correctness rate as a whole is significantly smaller in this dataset. This decrease is explained by the greater number of classes present in USPTex dataset, embarrassing the discrimination among so heterogeneous samples. The Fig. 5 depicts the correctness rate for the compared methods, when we vary the number of descriptors in the OuTex dataset. The result is similar to that of the other datasets and the best result is achieved through the Fourier method.

In the Table 1 we observe the best correctness rate achieved by each descriptor in the classification of Brodatz textures. The proposed Fourier fractal descriptor presents the greater correctness. Although it uses more descriptors than other techniques, the number of 74 descriptors does not compromise the computational cost of the classification process. We notice a significant advantage of Fourier descriptors of almost 40% relative to the second best method, that is, regularization. On the other hand, despite their reduced set of descriptors, the other fractal measures provided a very deficient result in the classification, even making impossible their application to practical situations. This behavior is observed in all tested data sets. (See Figs. 3–6.)

Here, it is also important to observe that the best precision in the estimation of the fractal dimension does not imply that such a method provides the best set of descriptors. Actually, methods like regularization dimension used to be more precise than the Fourier technique while the success rate of the descriptors has not expressed such a fact. This, in some sense, surprising result can be explained by the nature of the fractal descriptors approach. When we are dealing with a multiscale method, the information is not concentrated in the global measure (fractal dimension, in this case), but in each detail detectable at each level. Thus, even a method which captures faithfully the global fractality of the object can not be capable of discriminating effectively among different pixel patterns at different scales in the image. The distribution of such scale patterns is the key point for a good modeling of the analyzed object. The Table 2 shows the correctness rates for the usptex dataset. The behavior of each method is similar to that found in the Brodatz dataset, although the correctness is smaller for the compared methods, due to the grater number of classes in the dataset. The Table 3 shows the global correctness rate for each compared method in the OuTex dataset. One more time, the Fourier method presented the greater rate in the classification process. Although Brownian and Box-counting needed fewer descriptors for the best result, as can be seen in the Fig. 5, the increase in the number of descriptors does not imply an increase in the correctness rate and the global behavior is inferior to that of the proposed method. Finally, the Table 4 shows the global correctness for the leaves data set. Fourier presented a significant advantage of 25.7% over box-counting descriptors. Again, the Fourier method is demonstrated to be the best choice in this texture analysis task. In the following, we show the confusion matrices of the compared methods with best performances. The Fig. 7 shows the confusion matrix for each method in the Brodatz dataset. In the figures, the confusion matrix is depicted in 3D surfaces, in which each point corresponds to a specific column and

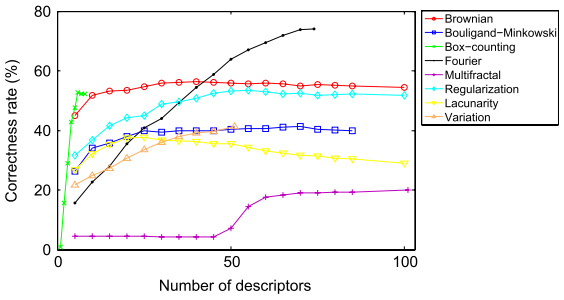

Fig. 3. Correctness rate for each descriptor method and number of descriptors in Brodatz dataset.

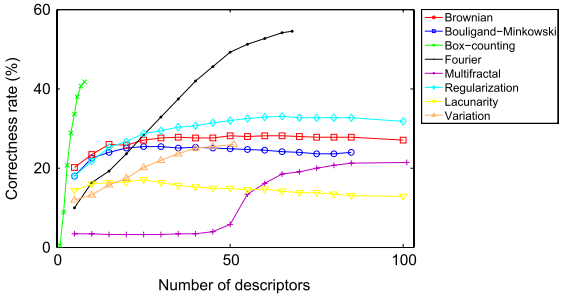

Fig. 4. Correctness rate for each descriptor method and number of descriptors in USPTex dataset.

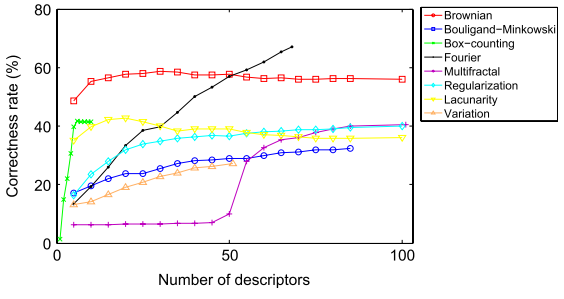

Fig. 5. Correctness rate for each descriptor method and number of descriptors in OuTex dataset.

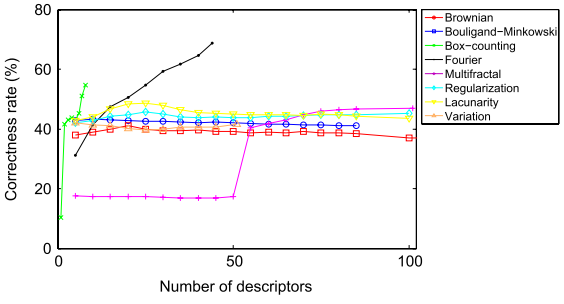

Fig. 6. Correctness rate for each descriptor method and number of descriptors in the plant leaves dataset.

line in the matrix and the height of the point corresponds to the value in the respective matrix. In these figures, the best methods must present higher regions in the principal diagonal. Besides, the points outside the diagonal must tend to present a smaller height. In this sense, the Fourier matrix presents the diagonal with more higher regions and the smaller number of lower points outside the diagonal. The Fig. 8 exhibits the confusion matrices for the USPTex dataset. Again, we observe the diagonal in the Fourier matrix with higher regions. The Fig. 9 shows the confusion matrices for the OuTex dataset. Again, the principal diagonal is more continuous with greater heights in the Fourier matrix. We can still observe that the pixels

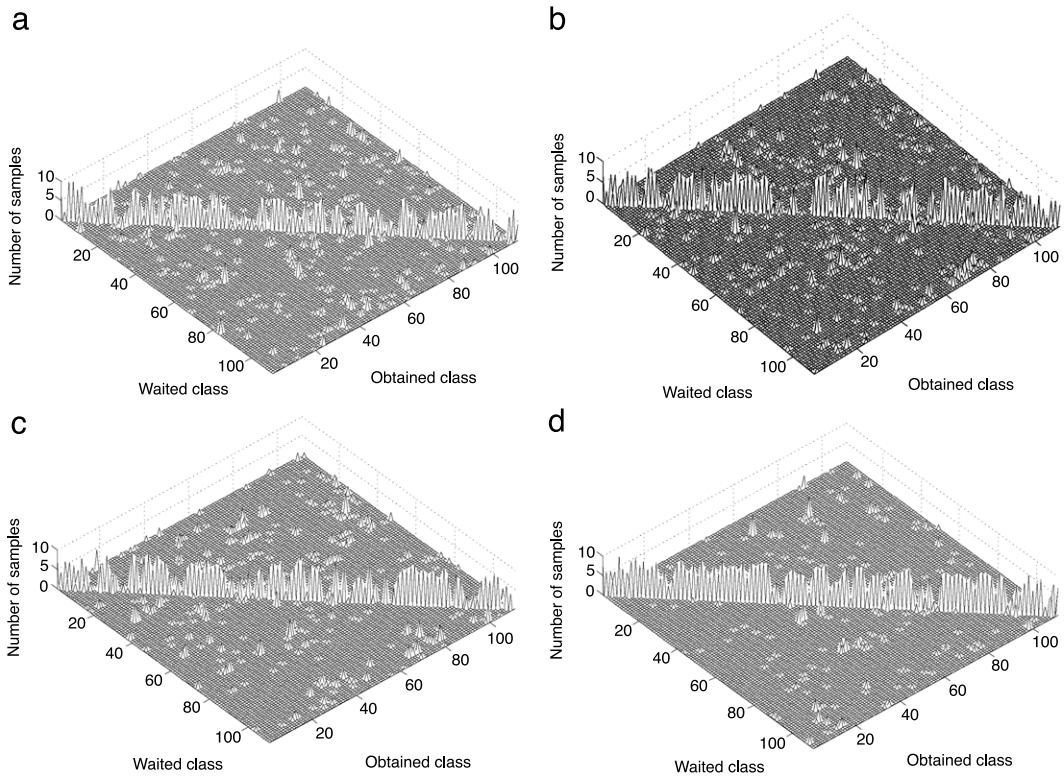

Fig. 7. Confusion matrices for each descriptor method in Brodatz dataset. Each matrix is mapped onto an image in where each value in the original image corresponds to a color in the image (see the colorbar legend). (a) Box-counting. (b) Regularization. (c) Brownian. (d) Fourier.

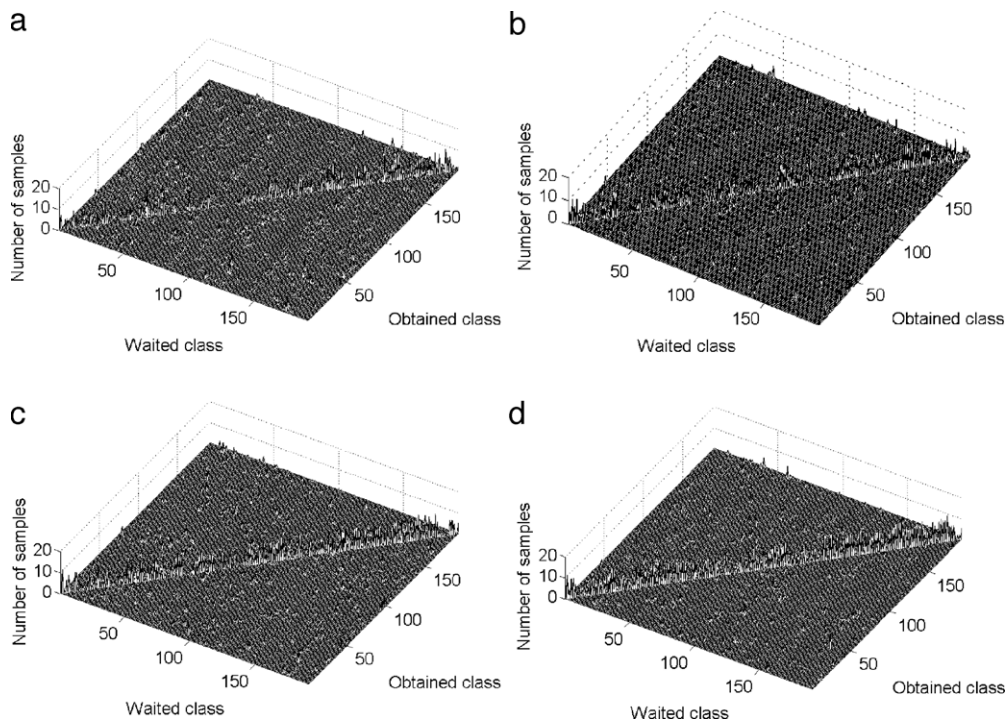

Fig. 8. Confusion matrices for each descriptor method in USPTex dataset. Each matrix is mapped onto an image in where each value in the original image corresponds to a color in the image (see the colorbar legend). (a) Brownian. (b) Regularization. (c) Box-counting. (d) Fourier.

Table 1
Correctness rate for the Brodatz dataset.

Method	Correctness Rate (%)	Number of descriptors
Minkowski	41.35	70
Brownian	56.31	40
Box-counting	52.70	6
Multifractal	35.86	85
Lacunarity measure	37.75	25
Regularization dimension	53.42	55
Variation dimension	41.26	51
Fourier	74.05	74

Table 2
Correctness rate for the USPTex dataset.

Method	Correctness Rate (%)	Number of descriptors
Minkowski	25.44	25
Brownian	28.14	65
Box-counting	41.67	8
Multifractal	21.34	101
Lacunarity measure	16.93	25
Regularization dimension	32.98	65
Variation dimension	25.96	51
Fourier	54.54	68

Table 3
Correctness rate for the OuTex dataset.

Method	Correctness Rate (%)	Number of descriptors
Minkowski	32.28	85
Brownian	58.60	30
Box-counting	41.62	6
Multifractal	40.44	101
Lacunarity measure	42.65	20
Regularization dimension	40.07	100
Variation dimension	27.21	51
Fourier	67.13	68

Table 4
Correctness rate for the plant leaves dataset.

Method	Correctness Rate (%)	Number of descriptors
Minkowski	43.23	10
Brownian	40.97	20
Box-counting	54.67	8
Multifractal	46.97	101
Lacunarity measure	48.72	25
Regularization dimension	45.64	25
Variation dimension	42.00	5
Fourier	68.72	4

with smaller heights outside the diagonal represent the misclassified samples. In the Fourier matrix, we observe that such lower points are less scattered and are nearer to the diagonal corresponding to a better precision in the discrimination of classes. The Fig. 10 shows the confusion matrices in the leaves experiment. One more time, in Fourier descriptors we have the higher regions on the principal diagonal. The other compared techniques present more elevation regions outside the diagonal, attesting to the presence of more severe misclassifications. In the Table 5 we present the average computational time (in seconds) expended by each one of the compared techniques in the calculus of descriptors from each image in the analyzed datasets. The advantage of the proposed Fourier technique is visible. Fourier is employed approximately only 14% of the time used by the Brownian descriptors, the second faster method.

8. Conclusions

The present work proposed the development and study of a novel texture descriptor based on the fractal dimension. Here, we proposed the use of Fourier fractal dimension to provide the descriptors. More specifically, the descriptors were obtained from the curve of Fourier power spectrum as a function of the frequency.

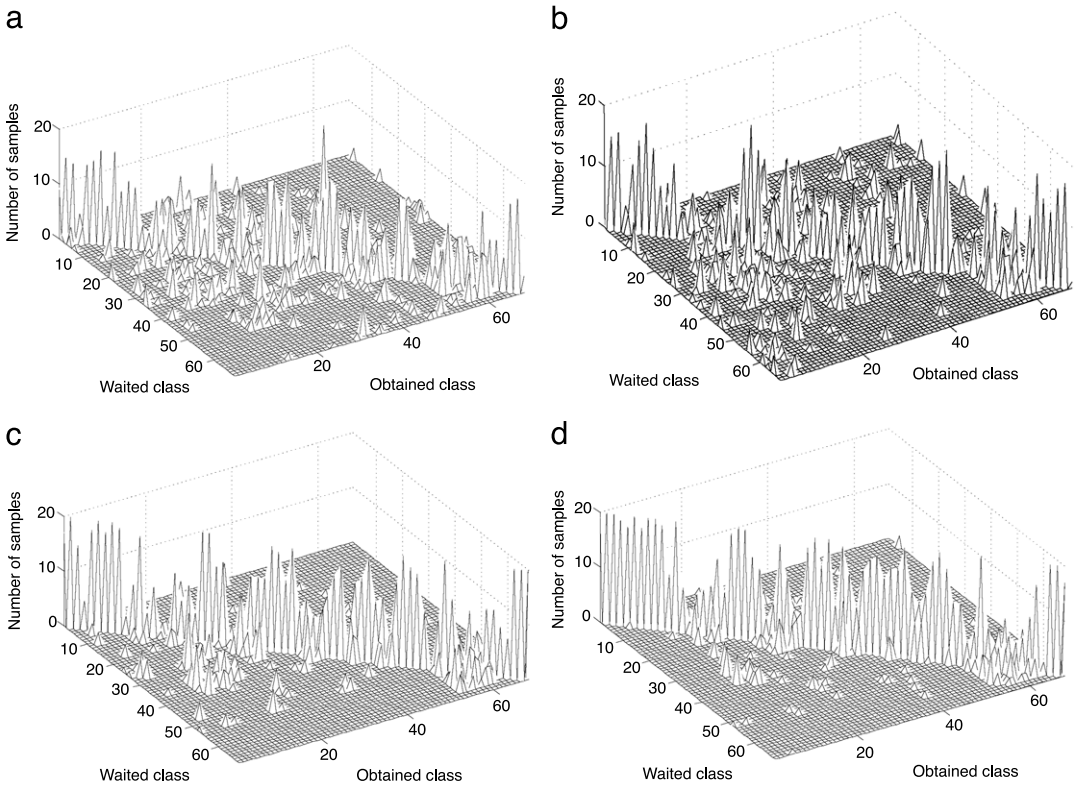

Fig. 9. Confusion matrices for each descriptor method in OuTex dataset. Each matrix is mapped onto an image where each value in the original image corresponds to a color in the image (see the colorbar legend). (a) Box-counting. (b) Lacunarity (c) Brownian. (d) Fourier.

Table 5
Average computational time used by each descriptor technique for each image in the tested datasets.

Method	Computational time (seconds)
Minkowski	3.72
Brownian	0.81
Box-counting	112.97
Multifractal	5.06
Lacunarity	0.16
Regularization	0.13
Variation	10.77
Fourier	0.03

The novel descriptors were compared to other approaches in which the descriptors are extracted from the fractal dimension, that is, the Bouligand–Minkowski, the box-counting, Brownian motion, multifractal, regularization, variation and lacunarity. The comparison was performed over two texture datasets, the Brodatz and the USPTex. The results were favorable to the proposed technique. Fractal Fourier descriptors presented the best correctness rate in the process of classification of textures based on the compared descriptors.

The achieved results suggest it is potentially an interesting technique which may be tested in applications relative to texture discrimination, in problems like classification, segmentation and general modeling of textures represented in digital images.

Acknowledgments

Odemir M. Bruno gratefully acknowledges the financial support of CNPq (National Council for Scientific and Technological Development, Brazil) (Grant #308449/2010-0 and #473893/2010-0) and FAPESP (The State of São Paulo Research Foundation) (Grant #2011/01523-1). João B. Florindo is grateful to CNPq(National Council for Scientific and Technological Development, Brazil) for his doctorate grant.

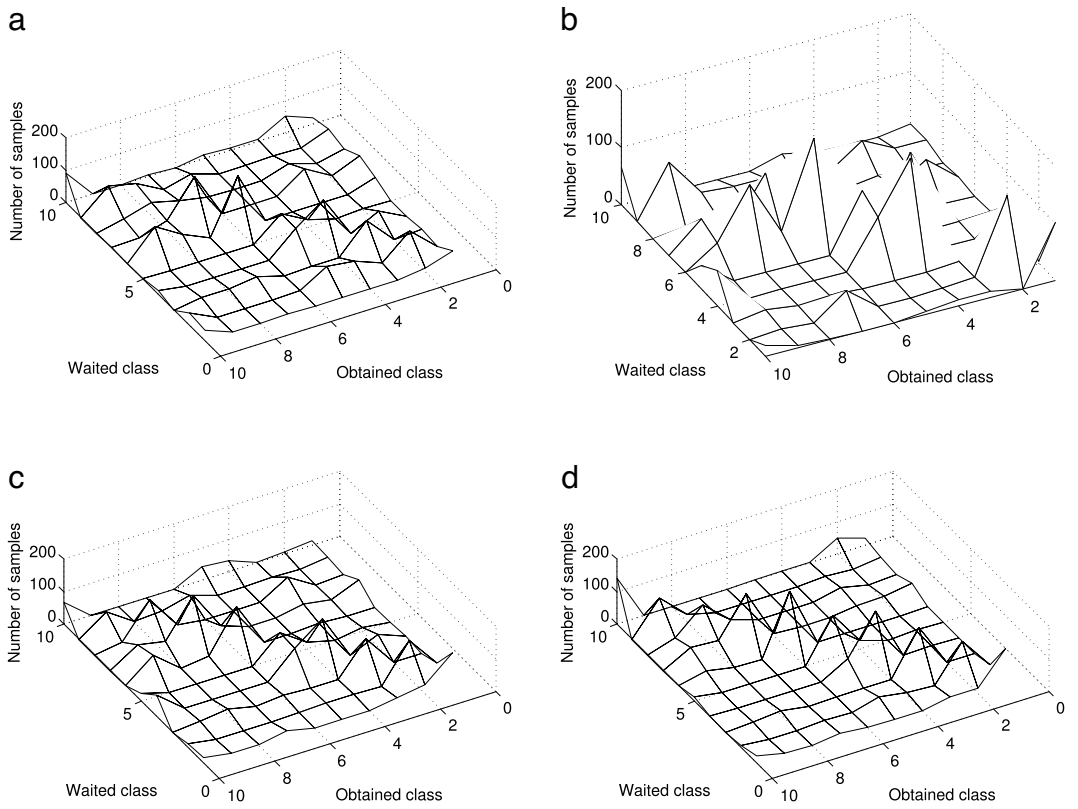

Fig. 10. Confusion matrices for each descriptor method in the leaves dataset. Each matrix is mapped onto a surface in which each value in the original matrix corresponds to a height in the surface (see the legend). (a) Multifractal. (b) Lacunarity. (c) Box-counting. (d) Fourier.

References

[1] B.B. Mandelbrot, The Fractal Geometry of Nature, Freeman, New York, 1968.
[2] M. Carlin, Measuring the complexity of non-fractal shapes by a fractal method, Pattern Recognition Letters 21 (11) (2000) 1013–1017.
[3] R.O. Plotze, J.G. Padua, M. Falvo, M.L.C. Vieira, G.C.X. Oliveira, O.M. Bruno, Leaf shape analysis by the multiscale Minkowski fractal dimension, a new morphometric method: a study in passiflora l. (passifloraceae), Canadian Journal of Botany-Revue Canadienne de Botanique 83 (2005) 287–301.
[4] D. Calzetti, M. Giavalisco, Fractal structures and the angular correlation function of galaxies, Vistas in Astronomy 33 (3/4) (1990) 295–304.
[5] A.L. Goldberger, Fractal electrodynamics of the heartbeat, in: J. Jalife (Ed.), Mathematical Approaches to Cardiac Arrhythmias, Vol. 591, New York Acad. Sci, New York, 1990, pp. 402–409.
[6] C. Tricot, Curves and Fractal Dimension, Springer-Verlag, 1995.
[7] J.C. Russ, Fractal Surfaces, Plenum Press, New York, 1994.
[8] E.T.M. Manoel, L.F. Costa, J. Streicher, G.B. Müller, Multiscale fractal characterization of three-dimensional gene expression data, in: SIBGRAPI, 2002, pp. 269–274.
[9] A.R. Backes, D. Casanova, O.M. Bruno, Plant leaf identification based on volumetric fractal dimension, International Journal of Pattern Recognition and Artificial Intelligence (IJPRAI) 23 (6) (2009) 1145–1160.
[10] A.R. Backes, O.M. Bruno, Shape classification using complex network and Multi-scale Fractal Dimension, Pattern Recognition Letters 31 (1) (2010) 44–51.
[11] R. Lopes, P. Dubois, I. Bhouri, M.H. Bedoui, S. Maouche, N. Betrouni, Local fractal and multifractal features for volumic texture characterization, Pattern Recognition 44 (8) (2011) 1690–1697.
[12] G. Neil, K. Curtis, Shape recognition using fractal geometry, Pattern Recognition 30 (12) (1997) 1957–1969.
[13] D. Chappard, I. Degasne, G. Hure, E. Legrand, M. Audran, M. Basle, Image analysis measurements of roughness by texture and fractal analysis correlate with contact profilometry, Biomaterials 24 (8) (2003) 1399–1407.
[14] Y. Xiang, V.R. Yingling, R. Malique, C.Y. Li, M.B. Schaffler, T. Raphan, Comparative assessment of bone mass and structure using texture-based and histomorphometric analyses, Bone 40 (2) (2007) 544–552.
[15] J. Veenland, J. Grashuis, E. Gelsema, Texture analysis in radiographs: the influence of modulation transfer function and noise on the discriminative ability of texture features, Medical Physics 25 (6) (1998) 922–936.
[16] O.M. Bruno, R. de Oliveira Plotze, M. Falvo, M. de Castro, Fractal dimension applied to plant identification, Information Sciences 178 (12) (2008) 2722–2733.
[17] J.B. Florindo, A.R. Backes, M. de Castro, O.M. Bruno, A Comparative Study on Multiscale Fractal Dimension Descriptors, Pattern Recognition Letters 33 (6) (2012) 798–806.
[18] L.F. Costa, R.M. Cesar Jr., Shape Analysis and Classification: Theory and Practice, CRC Press, Boca Raton, 2000.
[19] C.L. Jones, H.F. Jelinek, Wavelet packet fractal analysis of neuronal morphology, Methods 24 (4) (2001) 347–358.
[20] R.C. Gonzalez, R.E. Woods, Digital Image Processing, 2nd Edition, Prentice Hall, Boston, MA, USA, 2002.
[21] F. Galasso, J. Lasenby, Fourier analysis and gabor filtering for texture analysis and local reconstruction of general shapes, in: Proc. IEEE Conf. on Computer Vision and Pattern Recognition, CVPR, 2009, pp. 2342–2349.
[22] M.B. Ruskai, in: G. Beylkin, R. Coifman, I. Daubechies, S. Mallat, Y. Meyer, L. Raphael (Eds.), 1992: WTA, in: Wavelets and Their Applications, Jones and Bartlett, Boston, 1992.

[23] J.B. Florindo, M. De Castro, O.M. Bruno, Enhancing Multiscale Fractal Descriptors Using Functional Data Analysis, International Journal of Bifurcation and Chaos 20 (11) (2010) 3443–3460.
[24] A.P. Witkin, Scale space filtering: a new approach to multi-scale descriptions, in: Proceedings…, 2003, pp. 79–95.
[25] E.J. Weinberg, M.R.K. Mofrad, A multiscale computational comparison of the bicuspid and tricuspid aortic valves in relation to calcific aortic stenosis, Journal of Biomechanics 41 (16) (2008) 3482–3487.
[26] L. Angelini, R. Maestri, D. Marinazzo, L. Nitti, M. Pellicoro, G.D. Pinna, S. Stramaglia, S.A. Tupputi, Multiscale analysis of short term heart beat interval, arterial blood pressure, and instantaneous lung volume time series, Artificial Intelligence in Medicine 41 (3) (2007) 237–250.
[27] D. Marr, Vision: A Computational Investigation into the Human Representation and Processing of Visual Information, W. H. Freeman, San Francisco, 1982.
[28] P. Rosin, S. Venkatesh, Extracting natural scales using Fourier descriptors, Pattern Recognition 26 (9) (1993) 1383–1393.
[29] A.C. Bovik, M. Clark, W.S. Geisler, Multichannel Texture Analysis Using Localized Spatial Filters, IEEE Transactions on Pattern Analysis and Machine Intelligence 12 (1) (1990) 55–73.
[30] P. Brodatz, Textures: A Photographic Album for Artists and Designers, Dover Publications, New York, 1966.
[31] T. Ojala, T. Maenpaa, M. Pietikainen, J. Viertola, J. Kyllonen, S. Huovinen, Outex — New framework for empirical evaluation of texture analysis algorithms, in: 16th International Conference on Pattern Recognition, Vol I, Proceedings, 2002, pp. 701–706.
[32] R.O. Duda, P.E. Hart, Pattern Classification and Scene Analysis, Wiley, New York, 1973.
[33] M. Haridas, Introduction to weka: CIS764-step by step tutorial for weka (Aug. 14 2008).
[34] E. Chen, P. Chung, C. Chen, H. Tsai, C. Chang, An automatic diagnostic system for CT liver image classification, IEEE Transactions on Biomedical Engineering 45 (6) (1998) 783–794.
[35] U. Gonzales-Barron, F. Butler, Fractal texture analysis of bread crumb digital images, European Food Research and Technology 226 (4) (2008) 721–729.
[36] D. Harte, Multifractals: Theory and Applications, Chapman and Hall/CRC, New York, 2001.
[37] A.K. Jain, R.P.W. Duin, J. Mao, Statistical pattern recognition: A review, IEEE Transactions on Pattern Analysis and Machine Intelligence 22 (2000) 4–37.
[38] Y. Fisher, Fractal Image Encoding and Analysis: A NATO ASI Series Book, Springer-Verlag, New York, 1996.
[39] M.J. Turner, J.M. Blackledge, P.R. Andrews, Fractal Geometry in Digital Imaging, Academic Press, New York, 1998.
[40] M.P. Mäkynen, M.H. Similä, A.T. Manninen, M.T. Hallikainen, J.A. Karvonen, Dependence Between Standard Deviation and Measurement Length for C-Band Backscattering Signatures of the Baltic Sea Ice, IEEE transactions on geosciences and remote sensing 44 (10) (2006) 2890–2898.
[41] P.R. Bakic, D. Kontos, V. Megalooikonomou, M.A. Rosen, A.D.A. Maidment, Comparison of Methods for Classification of Breast Ductal Branching Patterns, in: IWDM 2006, LNCS, 2006, pp. 634–641.
[42] J.S. Torrecilla, E. ROJO, J.C. Dominguez, F. Rodriguez, A Novel Method To Quantify the Adulteration of Extra Virgin Olive Oil with Low-Grade Olive Oils by UV-Vis, J. Agric. Food Chem. 58 (2010) 1679–1684.
[43] O. Velazquez-Camilo, E. Bolaños-Reynoso, E. Rodriguez, J. Alvarez-Ramirez, Characterization of cane sugar crystallization using image fractal analysis, Journal of Food Engineering 100 (2010) 77–84.
[44] S. Ruzicka, P. Hausild, Fractal aspects of ductile and cleavage fracture surfaces, Engineering Fracture Mechanics 77 (2010) 744–752.
[45] J.L. Vehel, P. Legrand, Signal and Image processing with FracLab, in: Proc. of FRACTAL04, Complexity and Fractals in Nature, 8th International Multidisciplinary Conference, Vancouver, Canada, 2004.
[46] http://fraclab.saclay.inria.fr/homepage.html.